

# Binary random packing fraction of hyperspheres with small or large size difference: a geometric approach

H.J.H. Brouwers

Department of the Built Environment, Eindhoven University of Technology  
P.O. Box 513, 5600 MB Eindhoven, The Netherlands

Email:jos.brouwers@tue.nl

(Dated: January 27, 2025)

The random packing fraction of binary particles in  $D$ -dimensional Euclidean space  $\mathbb{R}^D$  is studied using a geometric approach. First, the binary packing fraction of assemblies with small size difference are studied, using the excluded volume model by Onsager for particles in three-dimensional space ( $D = 3$ ). According to this model the packing increase by bidispersity is proportional to  $(1 - f)(u^D - 1)^2$ , with  $f$  as monosized packing fraction,  $u$  as size ratio and  $D$  as space dimension. The model predictions are compared with computational results for disks in two dimensions ( $D = 2$ ) and hyperspheres in the large-dimension limit ( $D \rightarrow \infty$ ), yielding good agreement. Subsequently, the packing of hyperspheres with large size difference is modeled, employing the classic theory of Furnas. This theory, developed for three dimensions, starts from an infinite size ratio of larger and smaller particles ( $u \rightarrow \infty$ ). Here, the pertaining equations are applied to hyperspheres, and successfully compared with computational results for hyperspheres in the large-dimension limit. Furthermore, an asymptotic approximation of the binary packing fraction for large size ratio is derived, which shows that the first order variation of the Furnas packing fraction ( $u^{-1} = 0$ ) is proportional to  $(2 - f)u^{-1}$ . Finally, a scaled  $D$ -dimensional binary packing graph is presented, governing a simplified phase diagram that borders the binary random packing fraction of amorphous assemblies. To summarize, basic space-filling and geometric (“a-thermal”) theories on “simple” hard spheres appear to be a valuable tool for the study of hyperspheres’ packing and amorphization.

## 1. INTRODUCTION

The packing of particles is an old physical and mathematical puzzle and has received much attention the past millennia [1]. Attention has for instance been paid to revealing packing geometries and the route to understanding liquids and (amorphous) materials. Hard sphere systems are ideal to study liquid-glass-crystal transitions [2]. Furthermore, study of amorphous hyperspheres in  $D$ -dimensional space enables a better understanding of glass formation in three dimensions, and it brings the problem in contact with signal digitization and error coding theory [3].

When equally shaped particles with different sizes are randomly packed, *i.e.* generating a polydisperse packing of similar particles, the packing fraction increases compared to the monosized packing of the congruent (or identical) particles. Moreover, size dispersity frustrates crystallization and is therefore a glass phase enabler.

By combining two similar particles of different sizes, such a polydisperse packing can readily be assembled. In this paper this specific polydisperse particle packing is analysed, *viz.* the packing of two discretely sized and equally shaped particles, here termed bidisperse or binary mixtures. Though the binary packing of similar particles with a small size difference is a relatively simple polydisperse system, it forms the basis of the packing description of polydisperse arrangements. Early work on binary packings was for instance aimed on constructing packings of continuously sized particles with a wide size ratio [4-9].

The binary packing of similar particles was studied experimentally, computationally and analytically [10-32]. For binary mixes with size ratio  $u$  close to unity ( $u \downarrow 1$ ), analytical equations are available [18, 20, 29, 32]. Also, for the other limit, *viz.* infinite size ratio  $u$  ( $u \rightarrow \infty$ ), *i.e.* two noninteracting fractions, an analytical expression for the binary void fraction is available [4, 5], revisited later in [23, 26].

Here, in Section 2 first the model for binary particles with small size disparity is introduced [32], which was based on Onsager’s excluded volume model from 1949 [33]. Onsager developed this original geometric model for the isotropic liquid-to-nematic (L-N) phase transition of hard rodlike (spherocylinders and cylinders) particles, which was published in his seminal paper. Onsager demonstrated that a phase transition can be predicted based on two-particle (spherocylinders or cylinders) interactions represented by the second virial term in an expansion of the free energy of the system. Onsager based these expressions on the orientally averaged excluded volume of two (sphero)cylinders with unequal lengths and diameters. In essence this is an example of a statistical geometric approach. In [32], this excluded volume concept of two-particle pairs was combined with the statistically probable combinations of small and large particle pairs, yielding an analytical expression for the packing fraction of binary similar particles with small size disparity. This geometric approach of particle packing was successfully validated against a broad collection of computational and experimental data of packings in three dimensions. Here, this model is applied to binary disks in

plane and to binary hyperspheres with small size difference ( $u^D \downarrow 1$ ).

Next, in Section 3, the classic model of Furnas is recapitulated, which formulates the packing of particles with infinite size difference (or  $u^{-1} = 0$ ). About 100 years ago, Furnas [4, 5] introduced the concept of noninteracting particle classes, *i.e.* particle groups where the smallest particle of one group is much larger than the largest particle of the other group. Combining the groups implies that they are not interacting and forming separate phases. This geometric concept has been proven to be correct by experiments [4, 5, 9, 11] and simulations [23, 26, 28] in three dimensions. Here, we will apply this model to binary mixes of hyperspheres with infinite large size ratio. In Section 4, an asymptotic approximation of the bidisperse fraction is presented for large but finite size differences (so  $u^{-1} > 0$ ), that approaches the Furnas solution in the infinite size difference limit.

Subsequently, in Section 5 a generic graph is introduced of the scaled bidisperse packing fraction. This figure borders the scaled packing fraction of amorphous assemblies, as function of composition and from size ratios unity to infinity, and in the vicinity of these - opposite- limits. The conclusions are collected in Section 6.

The presented models provide the random or amorphous packing of nonoverlapping (*i.e.* hard) particles in the bidisperse case relative to the monodisperse case, in  $D$ -dimensional Euclidean space  $\mathbb{R}^D$ . They are applicable when the packing of the smaller and the larger particles, and their binary packing, are compacted equally. Whether the assembly's density corresponds to the glass transition density, maximum density, maximally random jammed state, random close packing (RCP), random loose packing (RLP) *etc.*, is inconsequential.

## 2. SMALL SIZE DIFFERENCE

This paper addresses the assemblies of binary (discretely sized) similar particles in  $D$ -dimensional space, the larger and smaller ones with characteristic sizes  $d_L$  and  $d_S$ , respectively, with a normalized number distribution

$$P(d) = X_S \delta(d - d_S) + X_L \delta(d - d_L) \quad , \quad (1)$$

where  $\delta$  is the Dirac delta function, and  $X_S$  and  $X_L$  are the number fractions of the smaller and larger components for which the following identity hold;

$$X_S + X_L = 1 \quad . \quad (2)$$

In this section the analytical model for binary mixtures with small size disparity [32] is recapitulated, and subsequently applied to binary hyperspheres in the large-dimension limit.

### 2.1 Analytical model

By employing the excluded volume model of Onsager [33], in [32] the following equation was derived for the random packing fraction of similar binary  $D$ -dimensional particles, assuming that mixes and two monodisperse assemblies possess same compaction, and a small size difference:

$$\eta(u^D \downarrow 1, X_L) = \frac{f(X_L(u^D - 1) + 1)}{X_L(u^D - 1) + 1 - X_L(1 - X_L)(1 - f)v(u^D)} \quad , \quad (3)$$

with  $u$  as size ratio  $d_L/d_S$  and as contraction function

$$v(u) = \frac{(u^D - 1)^2}{2(u^D + 1)} \quad (D = 2) \quad , \quad (4)$$

$$v(u^D) = \frac{4(u^D - 1)^2}{9(u^D + 1)} \quad (D \geq 3) \quad ,$$

and  $D$  as the space dimension. Eq. (3) reveals that the effect of bidispersity on packing fraction is governed by  $X_L(1 - X_L)(1 - f)v(u)$ . In [32] it was seen that for both RCP and RLP in  $\mathbb{R}^3$  these expressions are accurate up to  $u = 2$  or so, so a volume ratio  $u^D$  of about 8. In [32] it was furthermore postulated that this expression is also applicable to  $D \neq 3$ .

The large constituent number fraction is related to the large constituent volume fraction  $c_L$  by:

$$X_L = \frac{c_L}{(1 - c_L)u^D + c_L} \quad , \quad (5)$$

so that Eq. (3) can be written as

$$\eta(u^D \downarrow 1, c_L) = \frac{f(c_L(1 - u^D) + u^D)}{c_L(1 - u^D) + u^D - c_L(1 - c_L)(1 - f)v(u^D)} \quad . \quad (6)$$

Eqs. (3), (4) and (6) reveal that the increase in packing by binary dispersity is governed by volume ratio  $u^D$  (for  $D = 2$  it constitutes the surface area ratio) of the large and small particles, so the size ratio to the power dimension.

### 2.2 Disks in two dimensions

In this subsection Eqs. (4) and (6) are compared with simulation results of binary disks packed in two dimensions (*i.e.* Euclidean plane). A Monte Carlo-based compression program was employed by Wan and Yang [34] to simulate the binary packing fraction. Monte Carlo

methods have been extensively used in prior studies to investigate dense random packing structures. For instance, Chen et al. [35] generated truncated tetrahedra in maximally random jammed states using a sufficiently fast compression algorithm.

$c_L$	$\eta(u, c_L)$ $u = 1.4$	$\eta(u, c_L)$ $u = 1.7$	$\eta(u, c_L)$ $u = 2$	$\eta(u, c_L)$ $u = 3$
0.3	0.84529	0.84801	0.85129	0.86231
0.4	0.84532	0.84901	0.85285	0.86376
0.5	0.84586	0.85012	0.85412	0.86638
0.6	0.84590	0.85073	0.85520	0.86882
0.7	0.84563	0.85066	0.85504	0.86933
0.8	0.84522	0.84998	0.85324	0.86709
0.9	-	-	0.85104	0.85959

Table I Computationally generated binary packing fraction,  $\eta(u, c_L)$ , of binary disks ( $D = 2$ ) [34].

Meng et al. [36] produced dense random packings of monodisperse and binary spherocylinders by starting with configurations containing significant particle overlaps, followed by a relaxation algorithm. Wan and Yang [34] designed an algorithm based on fast compression that permits particle overlap, implemented using HOOMD-blue [37]. Specifically, they began with a random distribution of binary hard disks at a low packing fraction within a square box with periodic boundary conditions. A random compression factor between 0.9 and 1 was then selected, with which the box was compressed. If the resulting overlap, measured as the ratio of overlapping particles to the total particle count, was below 0.1, the compression was accepted, and overlaps were resolved using random Monte Carlo moves. Otherwise, the compression was rejected, and a new compression factor was chosen. This iterative process continued until dense packing configurations were achieved. In Table II the resulting packing fractions are included as function of size ratios  $u = 1.4, 1.7, 2$  and  $3$  and of large disk volume.

$X_L$	$c_L$ $u = 1.4$	$\eta(u, c_L)$ $u = 1.4$	$c_L$ $u = 1.7$	$\eta(u, c_L)$ $u = 1.7$
0.3	0.4565	0.84646	0.5533	0.85163
0.4	0.5665	0.84667	0.6583	0.85099
0.5	0.6622	0.84617	0.7429	0.84959
0.6	0.7462	0.84584	0.8126	0.84981
0.7	0.8206	0.84543	0.8709	0.84873

$X_L$	$c_L$ $u = 2$	$\eta(u, c_L)$ $u = 2$
0.3	0.6316	0.85417
0.4	0.7273	0.85411
0.5	0.8000	0.85340
0.6	0.8571	0.85196
0.7	0.9032	0.85026

Table II Computationally generated binary packing fraction,  $\eta(u, c_L)$ , of binary disks ( $D = 2$ ) [38].

Furthermore, binary disk packings are generated by Desmond [38], with the same algorithm reported in [21], but with a different energy minimizer. In Table II the generated packing fractions are tabulated for size ratios  $u = 1.4, 1.7$  and  $2$ , and for a number of number fractions  $X_L$ . With

$$c_L = \frac{X_L u^2}{1 + X_L (u^2 - 1)}, \quad (7)$$

the large disk surface fraction is computed and is included in Table II as well. Note that  $u^2$  is the surface area ratio of large and small disks.

The range of concentrations summarized in Tables I and II is such that the simulation protocols did not result in crystallization, which was found to be the case for lower and higher large disk fractions.

In Fig. 1, Eqs. (4) and (6), as well as the data of Tables I and II, are set out, scaled by a monosized packing fraction  $f$  of 0.8425. This value is based on fitting Eqs. (4) and (6) to the  $u = 1.4$  data from both [34] and [38], which result in the same  $f$ , and this aforementioned  $f$  lies in the range of reported values [39], and is close to the value of 0.844 reported in [21].

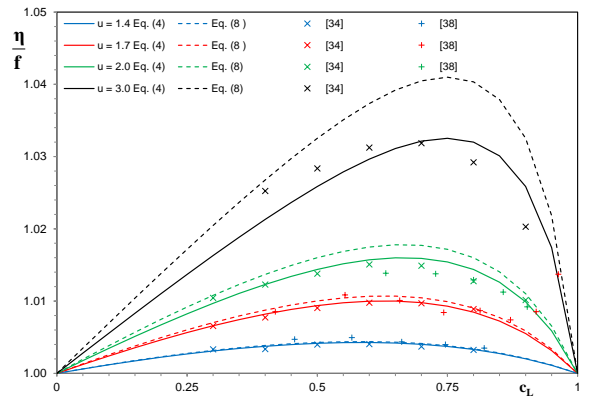


FIG. 1. Scaled packing fraction of binary disks,  $\eta(u, c_L)/f$ , for  $D = 2$ , using Eqs. (4) and (6), and the values of Tables I and II, using  $f = 0.8425$ .

The contraction function given by Eq. (4) follows from the combination of [10] and [33], and provided better predictions for larger  $u$  than the contraction function based on excluded volume only [32]. Fig. 1, also Eq. (6) with as alternative contraction function [32]

$$v(u) = (u - 1)^2, \quad (8)$$

is included. This function follows from the excluded volume model, and it converges to Eq. (4) for  $D = 2$  and  $u \downarrow 1$ .

Fig. 1 shows that the data generated by [34] and [38] are compatible with each other, and that Eqs. (4) and (6) match very well with these packing simulations. For  $u$

close to unity, the use of Eqs. (4) and (8) leads to almost identical  $\eta(u, c_L)/f$ , as expected, but for larger  $u$ , Eq. (8) tends to overestimate the binary packing fraction. The same trend was observed when applying the two different contraction functions to the packing of spheres in  $D = 3$  [32]. The presented comparison of simulations and model confirms that the excluded volume approach of Onsager is applicable to disks in  $D = 2$  and  $u$  up to 3 or so ( $u^D \approx 9$ ), and that contraction function Eq. (4) is most suitable indeed to capture the effect of size ratio on packing fraction for larger  $u$ . Also, the coefficient  $1 - f$  in Eqs. (3) and (6), which followed from the excluded volume model, is a major factor in this equation. For the considered two-dimensional packing its value ( $\approx 0.16$ ) is very distinct from the values pertaining to RLP ( $\approx 0.45$ ) or RCP ( $\approx 0.36$ ) of spheres packed in three dimensions [32]. As seen before in [32], the product of  $(1 - f)$  and Eq. (4) provides an accurate prediction of the packing increase by introducing bidispersity.

## 2.2 Hyperspheres in infinitely-large dimension

Binary mixtures of hyperspheres with  $D \rightarrow \infty$  were studied by Ikeda *et al.* [31], constructing a statistical mechanical mean-field theory, based on the replica liquid theory to determine the fluid-glass transition in high-dimensions. Interestingly, the mean-field number density corresponds to the average number of overlaps counted in the excluded volume [40]. The monosized packing fraction  $f$  of these hyperspheres tends to zero in the large-dimension limit, as  $f$  scales with  $2^{-D}$  [40-43], so

$$\lim_{D \rightarrow \infty} f = 0 \quad . \quad (9)$$

$c_L$	$\eta(u, c_L)/f$	$c_L$	$\eta(u, c_L)/f$
0	1	0.5487	1.01573
0.0487	1.00231	0.5973	1.01564
0.1018	1.00453	0.6504	1.0152
0.1504	1.00667	0.6991	1.0144
0.1947	1.00836	0.7478	1.01324
0.2478	1.01022	0.7965	1.01173
0.3009	1.01173	0.8496	1.0096
0.3496	1.01307	0.8982	1.00684
0.3982	1.01413	0.9469	1.00391
0.4469	1.01484	1	1
0.5000	1.01547	-	-

Table III Scaled binary packing fraction,  $\eta(u, c_L)/f$ , of binary hyperspheres ( $D \rightarrow \infty$ ), extracted from “Fig. 3” [31].

A scaling relation between size ratio  $u$  to the dimension  $D$  was introduced in [31] as follows

$$u = 1 + \frac{R}{D} \quad , \quad (10)$$

so that in the large-dimension limit holds

$$\lim_{D \rightarrow \infty} u^D = e^R \quad . \quad (11)$$

Ikeda *et al.* [31] provided data for  $R = 0.5$ , so  $u^D = \sqrt{e}$  ( $\approx 1.649$ ), which is smaller than 8, the limiting value for the model in  $D = 2$  and 3.

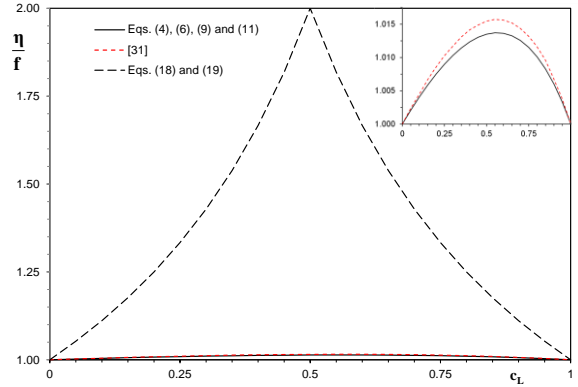


FIG. 2. Scaled packing fraction of binary hyperspheres,  $\eta(u, c_L)/f$ , for  $D \rightarrow \infty$ , using Eqs. (4), (6), (9) and (11), with  $R = 0.5$ , and Eqs. (18) and (19) for  $R \rightarrow \infty$  (equal to “Eqs. (27) and (28)” [31]). The pertaining computational results from “Fig. 3” of Ikeda *et al.* [31] are listed in Table III. Inset shows a magnified view of the same graph for small  $\eta(u, c_L)/f$ .

In Fig. 2, the scaled bimodal packing fraction,  $\eta(u, c_L)/f$ , following from Eqs. (4), (6), (9) and (11), is set out against the large hypersphere volume fraction  $c_L$ , employing this  $R = 0.5$ .

In this figure also the computational results from [31] are included, taken from “Fig. 3” (in which the scaled binary glass transition density is set out against small hypersphere volume fraction  $c_s$ , obviously  $c_L + c_s = 1$ ), and which values are listed in Table III. In Fig. 2 close agreement can be observed between the models presented here and in [31].

It appears that the results from statistical mechanical mean-field theory can also be explained with a geometric hard sphere packing model. Fig. 2 furthermore shows, as also found in [31], that though  $f$  is zero, the ratio  $\eta(u, c_L)/f$  is not.

## 3. LARGE SIZE RATIO

In this section the classic model of Furnas is revisited and applied to hyperspheres. This model provides closed-form expressions for binary particle mixes with infinite large size ratio ( $u \rightarrow \infty$ ).

### 3.1 Furnas model

Furnas [4, 5] studied binary systems in three dimensions and it was concluded that the greater the difference in size between the two components, the greater the decrease in void volume. For infinitely large size ratio, the small particles fill the voids of the large particles, and they form separate and noninteracting phases. For this situation Furnas provided closed-form expressions.

The underlying concept also applies to combinations of two particle types that have different monosized packing fractions [44], *e.g.* because their shape is different, their particle size distributions differ, the mode of compaction differs, *etc.* The concept is for instance also applicable to packings consisting of two continuously particle size distributions that are mixed [45].

The only prerequisite is that the packing assembly of the smaller constituent fits in the open space between the larger one. Here, we will restrict ourselves to two monodisperse constituents that possess an identical packing fraction, which is the case for similar particles that are assembled identically.

The volume fraction of the large constituent is defined as

$$c_L = \frac{V_L}{V_L + V_S} , \quad (12)$$

whereby for a binary packing fraction obviously holds

$$\eta(u, c_L) = \frac{V_L + V_S}{V_T} , \quad (13)$$

and where  $V_L$  and  $V_S$  are the volumes of the large and small constituents in the packing, respectively, and with  $V_T$  as total volume of the packing (entire space), including the voids.

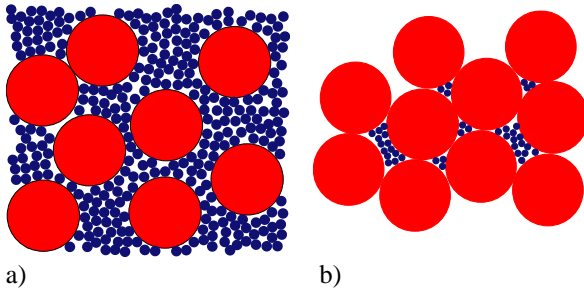


FIG. 3 Binary packing of noninteracting particles (a) Larger spheres (or disks in  $D = 2$ ) added to a monosized packing of smaller ones (b) Smaller spheres (or disks in  $D = 2$ ) added to a monosized packing of larger ones.

First, a monosized packing of small particles only is considered ( $c_L = 0$ ), in which large particles are introduced (Fig. 3a). This is the situation of a particle packing of small particles and their intermediate voids, total volume  $V_S/f$ , to which a volume  $V_L$  of large particles

is added. The binary packing fraction therefore reads as follows:

$$\eta(u \rightarrow \infty, c_L) = \frac{V_L + V_S}{V_L + V_S/f} = \frac{f}{1 - c_L(1 - f)} , \quad (14)$$

whereby Eq. (12) has been used.

Next, a packing of monosized large particles is considered, ( $c_L = 1$ ), total volume  $V_L/f$ , to which small particles are added (Fig. 3b). The binary packing fraction reads as follows

$$\eta(u \rightarrow \infty, c_L) = \frac{V_L + V_S}{V_L/f} = \frac{f}{c_L} , \quad (15)$$

where again Eq. (12) has been used. Eqs. (14) and (15) intersect when both the small and large particles have the monosized packing fraction. Furnas [4, 5] called mixes of binary particles that obey this composition “saturated mixtures”, and in such mixtures sufficiently small particles are added to just fill the void fraction between the large particles. Large and small particles form two separate phases that have the same packing fractions. For such saturated bidisperse packings, the volume fraction of the large fraction in the mix reads as follows:

$$c_L^{\text{sat}} = \frac{1}{2 - f} . \quad (16)$$

At this composition Eqs. (14) and (15) intersect, and

$$\frac{\eta^{\text{sat}}}{f} = 2 - f , \quad (17)$$

whereby  $\eta^{\text{sat}}$  stands for  $\eta(u \rightarrow \infty, c_L = c_L^{\text{sat}})$ , being the maximum for random binary packings or glasses. As this saturation point is the intersection of Eqs. (14) and (15), Eq. (14) is valid for  $0 \leq c_L \leq c_L^{\text{sat}}$ , and Eq. (15) for  $c_L^{\text{sat}} \leq c_L \leq 1$ . This saturation point can also be understood in another way: the large particles fill the total space with packing fraction  $f$ , and their voids are filled with the small particles’ packing that subsequently occupy  $(1 - f)f$  of the total space. Hence, both ingredients fill  $(2 - f)f$  of the total space (Eq. (17)) and the volume fraction of large particles,  $c_L$ , is  $(2 - f)^{-1}$  in this mix (Eq. (16)).

Obviously, this concept is applicable only when the smaller ones do not affect the packing of the larger size group. Experiments with mixtures of broken solids [4, 5] and steel balls [11] revealed that noninteraction between subsequent size groups is obviously true when  $u \rightarrow \infty$ , but that non-disturbance is also closely approximated when  $u \approx 7-10$ . For angular particles, Caquot [9] found empirically a comparable size ratio ( $u \approx 8-16$ ). Simulations showed that Eqs. (14) and (15) are approached closely for  $u = 10$  [23, 26].

### 3.2 Hyperspheres in infinitely-large dimension

The underlying concept, that the holes of the larger group are filled with the particles of the smaller groups, also holds for the  $D = 2$  case (circles in a plane), to which Fig. 3 also applies. This spatial or geometric concept holds for all particle shapes, and for all modes of packing, from RLP to RCP. Hence, it stands to reason that this geometric concept also holds in higher dimensions, that is for hyperspheres ( $D > 3$ ). This hypothesis is tested by an application to binary hyperspheres in the large-dimension limit, for which  $f = 0$  [40-43], see Eq. (9).

Hence, it follows from Eqs. (14)-(16) that  $c_L^{\text{sat}} = \frac{1}{2}$ , and that

$$\frac{\eta(u \rightarrow \infty, c_L)}{f} = \frac{1}{1 - c_L} \quad (0 \leq c_L \leq \frac{1}{2}), \quad (18)$$

$$\frac{\eta(u \rightarrow \infty, c_L)}{f} = \frac{1}{c_L} \quad (\frac{1}{2} \leq c_L \leq 1). \quad (19)$$

The first equation was presented as “Eq. (28)” in [31]:

$$\frac{\eta(u \rightarrow \infty, c_L)}{f} = \frac{1}{1 - c_L(1 - 2e^{-R/2})} \quad (0 \leq c_L \leq c_{L,\text{max}}) \quad (20)$$

if  $R \rightarrow \infty$  is applied, and Eq. (19) corresponds to “Eqs. (27)” [31]. The maximum packing fraction is attained at  $c_{L,\text{max}}$ , which equals  $c_L^{\text{sat}}$  for  $R \rightarrow \infty$ . Eq. (20) reveals that Eq. (14) is approximated with  $e^{-R/2}$ , so  $u^{-D/2}$  [31], see Eq. (11). In the next section this limit will be explored in more detail, there a detailed study is presented of the asymptotic behaviour of the binary packing fraction for large  $u$ .

The comparison with the results of [31] confirms the conjecture that the Furnas concept of noninteracting binary particles with large size ratio also holds for higher dimensions. Alternatively, one can say that the simulation results by Ikeda *et al.* [31] for binary hyperspheres can be explained by the classic geometric concept of Furnas, originally developed for particles in three dimensions. In Fig. 2, Eqs. (18) and (19) (or “Eqs. (27) and (28)” with applying  $R \rightarrow \infty$  [31]) are set out. Again, though  $f$  is zero, the ratio  $\eta(u^D, c_L)/f$  is not, and in the large-dimension and large size ratio limits, its maximum  $\eta^{\text{sat}}/f$  amounts to 2 at composition  $c_L^{\text{sat}} = \frac{1}{2}$  (Eqs. (16) and (17)).

### 4. ASYMPOTIC APPROXIMATION FURNAS MODEL

Eqs. (3), (4) and (6) reveal that near  $u = 1$  the binary packing varies with  $(u^D - 1)^2$ , this asymptotic behavior for  $u$  close to unity was discussed in detail in [32]. It is also interesting how the packing fraction approaches asymptotically the other limit, *viz.*  $u \rightarrow \infty$  or  $u^{-1} \downarrow 0$ . Here, the Furnas model is extended by providing an asymptotic

expansion of the binary packing fraction for  $u^{-1}$  tending to zero.

### 4.1 Large particles added to small particle packing

First, the following scaled binary packing fraction is introduced

$$\lambda(u, c_L) = \frac{\eta(u, c_L) - f}{\eta(u, c_L)(1 - f)} \quad (21)$$

In [32] it was shown that the RLP and RCP packing fractions of binary spheres with small size ratio collapse when scaled by Eq. (21). These RLP and RCP assemblies have a very distinct factor  $1 - f$  indeed (note that  $1 - f$  is the void fraction of the monosized packing fraction).

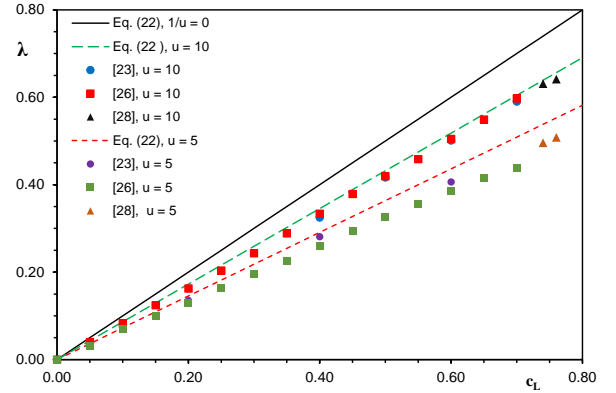


FIG. 4 Scaled binary random packing fraction  $\lambda(u, c_L)$  (defined by Eq. (21)) for  $D = 3$  as given by Eq. (22) for  $u = 5, 10$  and  $\infty$ , with  $\alpha = 1.365$  and  $\beta = 1$ , and the computational values provided by [23, 26, 28], listed in Tables IV, V and VI.

$c_L$	$\eta(u, c_L)$ $u = 5$	$\lambda(u, c_L)$ $u = 5$	$\eta(u, c_L)$ $u = 10$	$\lambda(u, c_L)$ $u = 10$
0	0.6435	0	0.6435	0
0.2	0.6761	0.135		
0.4	0.7152	0.281	0.7278	0.325
0.5			0.7557	0.416
0.6	0.7525	0.406	0.7835	0.501
0.7	0.7714	0.465	0.8150	0.590
0.75			0.8270	0.622
0.8	0.7769	0.482	0.7948	0.190
0.9	0.7111	0.267		
1	0.6435	0	0.6435	0

Table IV Binary packing fraction,  $\eta(u, c_L)$ , and scaled binary packing fraction,  $\lambda(u, c_L)$ , of binary spheres ( $D = 3$ ), with size ratios  $u = 5$  and  $10$ , taken from “Table I” [23]. The monosized packing fraction  $f$  is the value listed at  $c_L = 0$  and  $c_L = 1$  ( $f = 0.6435$ ).

In the previous section we have seen that in the large-dimension limit, in terms of  $\lambda$  (Eq. (21)), Ikeda *et al.* [31] proposed the following approximation

$$\lambda(u \rightarrow \infty, c_L) = c_L (1 - \alpha u^\beta) \quad (0 \leq c_L \leq c_{L,\max}), \quad (22)$$

with  $\alpha = 2$  and  $\beta = D/2$ , and which is based Eqs. (20) and (21). The large hypersphere volume fraction  $c_{L,\max}$  is the volume fraction at which the binary packing fraction reaches the maximum. Note that  $c_{L,\max}$  corresponds to  $c_L^{\text{sat}}$  for  $u \rightarrow \infty$ , for which  $(\lambda^{\text{sat}}, c_L^{\text{sat}}) = ((2 - f)^{-1}, (2 - f)^{-1})$ . For  $c_{L,\max} \leq c_L \leq 1$  no expansion of Eq. (19) in  $u$  was provided by [31].

The governing variable in the large size difference limit is the magnitude of the power  $\beta$ . The infinite size ratio limit of Furnas is approached when  $u \rightarrow \infty$ , in that case the size of the voids that contain the small particles is infinitely larger than the small particle size, and the small particles attain their infinite volume monosized packing fraction. This void (or container) size scales linearly with the large particle size.

The relation between container size and monosized packing fraction was already studied by Scott [5] for monosized spheres, who found that the infinite packing fraction is approached by  $u^{-1}$ . Desmond and Weeks studied the effect of container size on monosized packing fraction, both for  $D = 2$  (disks in  $\mathbb{R}^2$ ) and  $D = 3$  (spheres in  $\mathbb{R}^3$ ), also yielding a  $u^{-1}$  dependency.

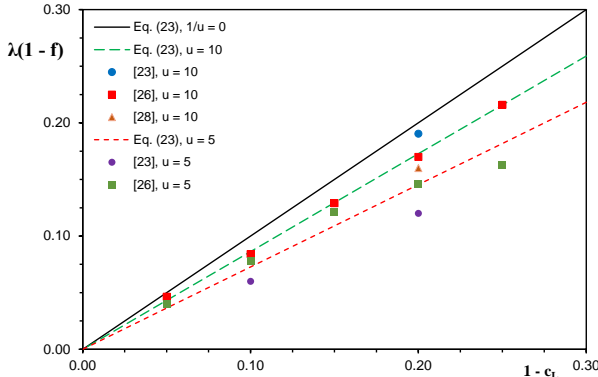


FIG. 5 Scaled binary random packing fraction  $\lambda(u, c_L)$  (defined by Eq. (21)) for  $D = 3$  as given by Eq. (23) for  $u = 5, 10$  and  $\infty$ , with  $\alpha = 1.365$ , and the computational values provided by [23, 26, 28], listed in Tables IV, V and VI.

Based on analogical reasoning, it is invoked that this dependency holds for all dimensions, so  $\beta = 1$ . Moreover, for  $u \rightarrow \infty$ , in Section 3 we have seen that this analogical reasoning also held when applying the noninteraction model of Furnas, which corresponds to  $u^{-1} = 0$ , to  $D \rightarrow \infty$ . The asymptotic behavior supposed here, proportional to  $u^{-1}$ , is different from [31], which derived a  $u^{-D/2}$  expansion. This latter expansion would imply that the Furnas limit can also be attained with a small size ratio  $u$  as long as  $D$  is large, which ignores the role of the size ratio.

The proposed asymptotic behavior towards the large size ratio limit is further analyzed by using the computational results of [23], [26] and [28], concerning spheres in three dimensions. In Tables IV, V and VI their binary RCP packing fraction results,  $\eta$ , for  $u = 5$  and  $10$  are summarized, as well as the pertaining  $\lambda$ .

In Fig. 4, Eq. (22) is set out for  $\alpha = 1.365$  (fitted) and  $\beta = 1$ , for  $u = 5, 10$  and  $\infty$ , as well as the data from Tables IV, V and VI concerning  $0 \leq c_L \leq c_{L,\max}$ . One can see that Eq. (22) with  $\alpha = 1.365$  and  $\beta = 1$  is able to capture the simulation results very well, especially for  $u = 10$ .

$c_L$	$\eta(u, c_L)$ $u = 5$	$\lambda(u, c_L)$ $u = 5$	$\eta(u, c_L)$ $u = 10$	$\lambda(u, c_L)$ $u = 10$
0	0.633	0	0.633	0
0.05	0.640	0.032	0.642	0.040
0.1	0.650	0.071	0.653	0.083
0.15	0.657	0.101	0.663	0.124
0.2	0.665	0.130	0.673	0.163
0.25	0.673	0.165	0.684	0.204
0.3	0.682	0.196	0.695	0.243
0.35	0.690	0.225	0.708	0.288
0.4	0.700	0.261	0.721	0.334
0.45	0.709	0.294	0.735	0.379
0.5	0.719	0.325	0.748	0.419
0.55	0.728	0.355	0.761	0.458
0.6	0.738	0.387	0.777	0.505
0.65	0.746	0.415	0.793	0.549
0.7	0.754	0.438	0.810	0.597
0.75	0.756	0.163	0.807	0.216
0.8	0.741	0.146	0.762	0.170
0.85	0.720	0.121	0.727	0.129
0.9	0.686	0.078	0.691	0.084
0.95	0.659	0.040	0.664	0.046
1	0.633	0	0.633	0

Table V Binary packing fraction,  $\eta(u, c_L)$ , and scaled binary packing fraction,  $\lambda(u, c_L)$ , of binary spheres ( $D = 3$ ), with 2 different size ratios  $u$ , extracted from “Fig. 2” [26]. The monosized packing fraction  $f$  is the value listed at  $c_L = 0$  and  $c_L = 1$  ( $f = 0.633$ ).

$c_L$	$\eta(u, c_L)$ $u = 5$	$\lambda(u, c_L)$ $u = 5$	$\eta(u, c_L)$ $u = 10$	$\lambda(u, c_L)$ $u = 10$
0.74	0.775	0.496	0.824	0.824
0.76	0.779	0.508	0.829	0.829
0.80			0.779	0.160

Table VI Binary packing fraction,  $\eta(u, c_L)$ , and scaled binary packing fraction,  $\lambda(u, c_L)$ , of binary spheres ( $D = 3$ ), with 2 different size ratios  $u$ , extracted from “Fig. 6” [28]. The monosized packing fraction  $f = 0.634$  [28].

Hence, the asymptotic expansion proposed by Ikeda *et al.* [31], based on  $D \rightarrow \infty$ , is also applicable to  $D = 3$ . The fitted value of  $\alpha$  is such that it equals  $2 - f$  considering that  $f \approx 0.635$  for RCP of spheres in  $D = 3$ . This relation between  $\alpha$  and  $f$  is furthermore supported by  $\alpha = 2$  for  $D \rightarrow \infty$ , see Eq. (20), since then  $f = 0$ .

## 4.2 Small particles added to large particle packing

The computational results of [23], [26] and [28] also enable an analysis of the asymptotic behavior for  $c_{L,\max} \leq c_L \leq 1$ . In Fig. 5,  $\lambda(u, c_L)(1-f)$  instead of  $\lambda(u, c_L)$  is set out for  $c_{L,\max} \leq c_L \leq 1$ , the values again taken from Tables IV, V and VI. For this latter range,  $\lambda(u, c_L)(1-f)$  is set out, as then the different monosized packing fractions, *viz.* 0.6435 [23], 0.633 [26] and 0.634 [28], can be accounted for.

Hence, in terms of  $\lambda$ , the approximation of Eq. (19) is written as

$$\lambda(u \rightarrow \infty, c_L)(1-f) = (1 - c_L)(1 - \alpha u^{-1})$$

$$(c_{L,\max} \leq c_L \leq 1) , \quad (23)$$

so asserting a similar asymptotic behavior as in the concentration range  $0 \leq c_L \leq c_{L,\max}$ .

In Fig. 5, Eq. (23) is displayed, again using  $\alpha = 1.365$ , and the data from Tables IV, V and VI concerning  $c_{L,\max} \leq c_L \leq 1$ , so invoking the same values for  $\alpha$  and  $\beta$  as in the range  $0 \leq c_L \leq c_{L,\max}$ . Though the number of data points is less and more dispersed, we can see that Eq. (23) is able to capture the asymptotic behavior in this concentration range for  $u \geq 10$  well, and that again the value of  $\alpha = 1.365$  provides good agreement.

## 4.3 Expanded Furnas model

The previous analysis allows for new expressions for the Furnas limit as function of size ratio  $u$ . Based on the above analysis of  $\lambda$ , asymptotic approximations for the binary packing fraction  $\eta$  of spheres RCP for small  $u^{-1}$  are obtained by transforming scaled packing fraction  $\lambda$  back to the binary packing fraction  $\eta$ , using the inverse of Eq. (21):

$$\eta(u, c_L) = \frac{f}{1 - \lambda(u, c_L)(1-f)} . \quad (24)$$

Substituting Eqs. (22) and (23) yield

$$\eta(u \rightarrow \infty, c_L) = \frac{f}{1 - c_L(1-f)(1 - (2-f)u^{-1})}$$

$$(0 \leq c_L \leq c_{L,\max}) , \quad (25)$$

applicable from  $u = 10$  to  $\infty$ , and perhaps even from  $u = 5$  to  $\infty$ , and

$$\eta(u \rightarrow \infty, c_L) = \frac{f}{1 - (1 - c_L)(1 - (2-f)u^{-1})}$$

$$(c_{L,\max} \leq c_L \leq 1) , \quad (26)$$

applicable from  $u = 10$  to  $\infty$ , whereby  $f = 0.635$ . One can recognize the similarity between Eq. (20) (or “Eq. (28)” of [31]) and Eq. (25) when  $f = 0$  (which is the case for  $D \rightarrow \infty$ ) and that here the expansion follows  $u^{-1}$  instead of  $u^{-D/2}(e^{-R/2})$ , as discussed before.

Obviously Eqs. (25) and (26) tend to the original equations of Furnas, Eqs. (14) and (15), respectively, for  $u^{-1} \downarrow 0$ , so  $u \rightarrow \infty$ . Eqs. (25) and (26) allow for an assessment of the bidisperse packing fraction for small  $u^{-1}$ , from 0 up to 0.1 or so. In other words, they are applicable to large but finite values of  $u$  (*i.e.*  $u > 10$ ).

For  $D = 3$ ,  $\alpha = 1.365$  and  $\beta = 1$  are appropriate values for RCP of spheres. The expressions might also be applicable for other particle shapes and other dimensions  $D$  if  $\alpha$  would equal  $2 - f$  indeed. This conjecture is supported by the large-dimension limit findings, for which  $\alpha = 2$  and  $f = 0$ .

## 5. BINARY RANDOM PACKING DIAGRAM

In the previous sections it was seen that the binary random packing fraction can be described with the same equations for all  $D$ , *viz.* Eqs. (4) and (6) for  $u^D \downarrow 1$ , and Eqs. (25) and (26) for  $u \rightarrow \infty$ . In this section a general binary packing fraction graph in  $\mathbb{R}^D$  is presented, using the suitable scaled binary random packing fraction  $\lambda$  (Eq. (21)).

### 5.1 Boundaries

By using Eq. (21), the binary packing fraction for  $u^D \downarrow 1$ , Eq. (6), can be expressed in  $\lambda(u^D, c_L)$  as follows

$$\lambda(u^D \downarrow 1, c_L) = \frac{c_L(1 - c_L)v(u^D)}{c_L(1 - u^D) + u^D} . \quad (27)$$

This scaled binary packing fraction does no longer contains the monosized packing fraction  $f$ .

In Fig. 6 this scaled packing fraction is included for  $u^D = 8$  and using Eq. (4), *e.g.* the case of packed disks in  $\mathbb{R}^2$  for which  $u = 2\sqrt{2}$ , or spheres in  $\mathbb{R}^3$  for which  $u = 2$ , the latter case being analyzed in [32].

In contrast to  $\lambda(u \rightarrow \infty, c_L)$ ,  $\lambda(u^D \downarrow 1, c_L)$  does not depend on the monosized packing fraction  $f$ , it is governed by  $u^D$  and composition  $c_L$  only. On the other hand, towards large  $u$ , the packing fraction depends on monosized packing fraction  $f$  (which in turn depends on  $D$ ) and composition  $c_L$  only, see Eqs. (22) and (23).

Fig. 6 therefore is a simplified graph of the full range of all possible amorphous binary particle packing fractions, applicable to all  $\mathbb{R}^D$ , particle types and densification (from RLP to RCP), as function of composition and size ratio. For  $u \rightarrow \infty$ , the upper boundary lines result from Eqs. (22) and (23) and these lines form a triangle. The top of the triangle is termed  $\lambda^{\text{sat}}$ , which follows from Eqs. (17) and (21) as

$$\lambda^{\text{sat}} = \frac{1}{2 - f} \quad . \quad (28)$$

The coordinates of this top are therefore  $(c_L^{\text{sat}}, \lambda^{\text{sat}}) = ((2 - f)^{-1}, (2 - f)^{-1})$ . Remarkably, the scaled packing fraction is thus bound by two lines defined by  $2 - f$ . The shaded area covers the range of possible binary packing fractions, which depend on composition  $c_L$  and size ratio  $u$  only. The maximum achievable scaled packing fraction,  $(c_L^{\text{sat}}, \lambda^{\text{sat}}) = ((2 - f)^{-1}, (2 - f)^{-1}) \approx (0.733, 0.733)$ , is indicated.

As observed before, for  $f = 0$  (which is the case for  $D \rightarrow \infty$ ) and  $u^{-1} = 0$  ( $u \rightarrow \infty$ ), Eqs. (22) and (23) form an isosceles triangle, with  $(c_L^{\text{sat}}, \lambda^{\text{sat}}) = (1/2, 1/2)$  as maximum scaled packing. The height from horizontal base to apex is thus  $1/2$ . In the  $\eta(u, c_L)$  graph, the upper boundary is then formed by two convex curves (Fig. 2), see Eqs. (18) and (19), that are reflectionally symmetrical with respect to vertical line  $c_L = 0.5$ .

## 5.2 Extrema

Towards  $u \downarrow 1$ , the extremum of Eq. (27) follows from the partial derivative of  $\lambda(u^D, c_L)$ , with respect to  $c_L$ :

$$\lambda_{C_L}(u^D \downarrow 1, c_L) = \frac{(u^D(1-c_L)^2 - c_L^2)v(u^D)}{(c_L(1-u^D) + u^D)^2} \quad . \quad (29)$$

Equating Eq. (29) to zero yields the large particle volume fraction  $c_{L,\max}$  which results in the maximum packing for a given size ratio  $u$  and dimension  $D$ :

$$c_{L,\max} = \frac{u^{D/2}}{u^{D/2} + 1} \quad . \quad (30)$$

For  $u^D \downarrow 1$ , this maximum packing fraction is located at  $c_{L,\max} = \frac{1}{2}$ . It also follows that  $c_{L,\max}$  is larger than  $\frac{1}{2}$  for  $u^D > 1$ . This can be seen in Figs. 2 (line  $u^D = e^R = \sqrt{e}$ , inset) and 6 (line  $u^D = 8$ ). Eq. (30) also follows from determining the maximum of Eq. (6), that is by differentiating with respect to  $c_L$  and equating the derivative to zero. So, the maximum of  $\lambda(u^D, c_L)$  and of  $\eta(u^D, c_L)$  are located at the same  $c_{L,\max}$ . The maximum binary packing fraction therefore follows from substituting Eq. (30) into Eq. (6), producing

$$\frac{\eta_{\max}(u)}{f} = \frac{(1-u^D)(1+u^{D/2}) + u^{D/2}(1+u^{D/2})^2}{(1-u^D)(1+u^{D/2}) + u^{D/2}(1+u^{D/2})^2 - (1-f)v(u^D)}, \quad (31)$$

and the maximum of the scaled binary packing fraction follows from substituting Eq. (30) in Eq. (27), yielding

$$\lambda_{\max}(u) = \frac{v(u^D)}{(u^{D/2} + 1)^2} \quad . \quad (32)$$

For the other limit, the asymptotic approximations are such that the volume fraction at maximum packing,  $c_{L,\max}$ , is  $c_L^{\text{sat}}$  (Eq. (16)) for  $u^{-1} < 0.1$  ( $u > 10$ , so not  $u \rightarrow \infty$  only). This particular follows from the intersection of Eqs. (25) and (26). At this  $c_{L,\max}$ , the maximum packing fraction amounts to

$$\eta_{\max}(u \rightarrow \infty) = \frac{f(2-f)}{1 + (1-f)(2-f)u^{-1}} \quad , \quad (33)$$

which is the packing fraction at the intersection of Eqs. (25) and (26), and there the scaled maximum packing fraction amounts to

$$\lambda_{\max}(u \rightarrow \infty) = \frac{1 - (2-f)u^{-1}}{2-f} , \quad (34)$$

which the intersection of the lines given by Eqs. (22) and (23) at  $c_{L,\max} = c_L^{\text{sat}}$ , and when  $\alpha$  is taken to be  $2 - f$  and  $\beta = 1$ . For  $u \rightarrow \infty$ ,  $\lambda_{\max}$  is  $\lambda^{\text{sat}}$ , and as concluded before, it appears that the values of  $\lambda^{\text{sat}}$  and  $c_L^{\text{sat}}$  are then the same, namely  $(2 - f)^{-1}$ , see Eq. (16) and Fig. 6.

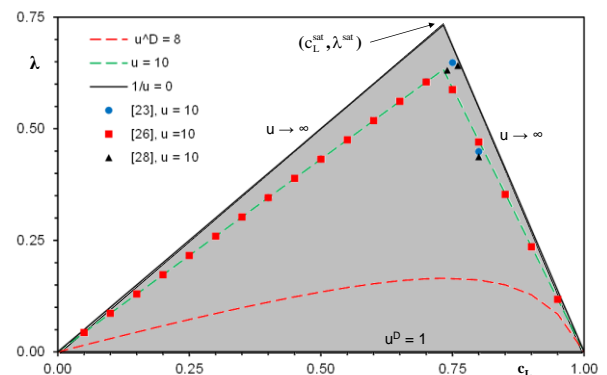


FIG. 6 Scaled binary random packing fraction  $\lambda(u, c_L)$  (defined by Eq. (21)) for  $u = 10$  and  $u \rightarrow \infty$  (Eqs. (25) and (26)), for  $u^D = 8$  (Eqs. (4) and (6)) and taking  $f = 0.635$ ,  $(c_1^{\text{sat}}, \lambda^{\text{sat}}) = ((2-f)^{-1}, (2-f)^{-1}) \approx (0.733, 0.733)$ .

In Fig. 6, Eqs. (22) and (23) are set out with  $\alpha = 2 - f$  and  $\beta = 1$ , and taking  $f = 0.635$  as example, for  $u = 10$  and  $u = \infty$ , and the maxima can be seen.

Interestingly, for  $f = 0$ ,  $c_{L,\max}$  is  $1/2$  for  $u^D = 1$ , then increases for  $u^D > 1$ , and for larger  $u^D$  it returns to  $1/2$  again for  $u$  larger than 10 or so. Also for  $f > 0$  one can observe that  $c_{L,\max}$  first increases with  $u$  increasing from unity ([11], [23] and [26]), and then decreases to  $c_L^{\text{sat}}$  when  $u$  exceeds 10. For these cases this trend in  $c_{L,\max}$  eccentricity is more difficult to recognize than for  $f = 0$ , *i.e.* in the large-dimension limit.

## 6. CONCLUSION

This paper addresses the problem of random packing fraction, or glass transition, of binary similar particles,

with small size difference ( $u$  near unity) and large size difference ( $u^{-1}$  near zero), and in variety of Euclidean spaces ( $D = 2, 3$  and  $\infty$ ), with emphasis on hyperspheres. First, small size difference ( $u$  close to unity) is studied. The model of [32], derived by combining Onsager's excluded volume model of particle pairs [33], and their statistical occurrence, can be successfully applied to both binary disks in  $\mathbb{R}^2$ , and to hyperspheres in the large-dimension limit. The approach is validated using the results of the computational studies by [31], [34] and [38]. Subsequently, the opposite limit, infinite large size difference, is addressed. Here, the classic geometric model of Furnas is recapitulated. Furnas [4, 5] studied bidisperse mixtures of particle groups with constituents that have an infinitely-large size disparity  $u$ . It is successfully demonstrated that this concept is also applicable to binary hyperspheres in the large-dimension limit, again using the computational results of [31]. An original model is proposed for the asymptotic approximation of the Furnas limit, so for  $u^{-1} \downarrow 0$ . It is reasoned that in all dimensions this approximation should follow  $u^{-1}$ . Based on the packing fraction of spheres in  $D = 3$  and hyperspheres in  $D \rightarrow \infty$ , there is sufficient evidence that the coefficient in the asymptotic approximation is  $2 - f$ . New expression for the binary packing fraction for large size ratio  $u$  are put forward, Eqs. (25) and (26), that converge to the Furnas expressions, Eqs. (14) and (15), for  $u \rightarrow \infty$ .

Finally, a packing graph of the scaled binary packing fraction  $\lambda(u, c_L)$  is constructed (Fig. 6), featuring the limits of the amorphous state of  $D$ -dimensional binary packings as a function of a reduced number of parameters. This scaled packing fraction was introduced in [32] and does, in contrast to the binary packing fraction  $\eta(u, c_L)$ , not depend on monosized packing fraction  $f$  anymore for  $u^D$  close to unity. Furthermore, for  $u^1$  close to zero,  $\lambda(u, c_L)$  depends linearly on  $c_L$ , whereas original packing fraction  $\eta(u, c_L)$  is a convex function.

This  $\lambda(u, c_L)$  figure features the saturated composition,  $c_L = c_L^{\text{sat}}$ , which constitutes a special mix where the concentrations of large and small fractions are such that the small particles packing fits in the voids of the large particles packing (Fig. 3) and hence they form separate phases that have the same packing fraction. It also represents the maximum attainable binary packing

fraction. It appears that the values of  $\lambda^{\text{sat}}$  and  $c_L^{\text{sat}}$  are the same, namely  $(2 - f)^{-1}$ , and these values characterize the graph (e.g. Fig. 6). In this graph, the upper boundaries belonging to  $u^{-1} = 0$ , being straight lines, are approached asymptotically by the term  $(2 - f)u^{-1}$ , and the horizontal base line pertaining to  $u^D = 1$  is asymptotically approached by  $(1 - f)(u^D - 1)^2$  with  $u^D$  as volume ratio (surface ratio in  $\mathbb{R}^2$ ) of the bidisperse particles.

The packing fraction of the two monodisperse components, and of their bidisperse mix, depends on the compaction, which are asserted all to be identical. This compaction may correspond to the glass (transition) density, maximum density, maximally random jammed, RCP, RLP etc.. The present model for the binary packing fraction can cope with all states of compaction, *i.e.* they all feature the same binary packing fraction divided by monosized packing  $(\eta(u, c_L)/f)$ . Though in the large-dimension limit the monodisperse packing fraction  $f$  tends to zero,  $\eta(u, c_L)/f$  attains a finite value.

Hence, it appears that the packing fraction of the binary mix depends on the monosized packing fraction  $f$ , space dimension  $D$ , composition  $c_L$  and size ratio  $u$ . In the small size disparity limit it depends on volume ratio  $u^D$ , and towards infinite size difference it depends on inverse size ratio  $u^{-1}$ .

Noteworthy, the used models are based on physical principles, and no adjustable parameter needed to be introduced to achieve the presented results. Concluding, one can say that the results of this study are a strong support for the applicability and validity of analytical "simple" and "athermal" hard hypersphere packing models, based on statistical geometry, to describe the amorphous states of soft condensed matter.

## ACKNOWLEDGEMENTS

Dr. D.D. Wan and Mr. Y.H. Yang (Wuhan University), and Dr. K.W. Desmond (Emory University), are acknowledged for providing computer simulations of binary disk packings (Tables I and II, respectively). Dr. F. Zamponi (Sapienza University) is thanked for the discussions and providing Ref. [31]. Dr. Yan Luo is acknowledged for extracting the data of Refs. [26], [28] and [31], displayed in Figs. 2, 4, 5 and 6. Mrs. Yilu Chen is thanked for assisting in the drawing Fig. 3.

---

[1] S. Torquato and F.H. Stillinger, Rev. Mod. Phys. 82, 2633 (2010).  
[2] G. Parisi and F. Zampini, Rev. Mod. Phys. 82, 789 (2010).  
[3] P. Charbonneau, A. Ikeda, A., G. Parisi, G. and F. Zamponi, Phys. Rev. Lett. 107, 185702 (2011).  
[4] C.C. Furnas, Department of Commerce, Bureau of Mines, Report of Investigation Serial No. 2894 (1928).  
[5] C.C. Furnas; Bulletin of US Bureau of Mines 307, 74 (1929).  
[6] A.E.R. Westman and H.R. Hugill, J. Am. Ceram. Soc. 13, 767 (1930).  
[7] C.C. Furnas, Ind. Eng. Chem. 23, 1052 (1931).  
[8] A.E.R. Westman, J. Am. Ceram. Soc. 19, 127 (1936).  
[9] M.A. Caquot, Mémoires de la Société des Ingénieurs Civils de France, 562 (in French) (1937).

[10] P.C. Mangelsdorf and E.L. Washington, *Nature*, Lond. 187, 930 (1960).

[11] R.K. McGahey, *J. Am. Ceram. Soc.* 44, 513 (1961).

[12] R. Jeschar, W. Pötke, V. Petersen and K. Polthier, *Proceedings Symposium on Blast Furnace Aerodynamics*, Wollongong, Australia, 25th-27th September 1975, Ed. N. Standish, pp. 136-147, Illawara Branch of the Australasian Institute of Mining and Metallurgy (Aus. I.M.M.) (1975).

[13] A.S. Clarke and J.D. Wiley, *Phys. Rev. B* 35, 7350 (1987).

[14] A.P. Shapiro and R.F. Probstein, *Phys. Rev. Lett.* 68, 1422 (1992).

[15] A. Yang, C.Y. Miller and L.D. Turcoliver, *Phys. Rev. E* 53, 1516 (1996).

[16] D. He, N.N. Ekere and L. Cai, *Phys. Rev. E* 60, 7098 (1999).

[17] H.J.H. Brouwers, *Phys. Rev. E* 74, 031309, *ibid* 069901 (E) (2006), *ibid E* 84, 059905 (E) (2011).

[18] H.J.H. Brouwers, *Phys. Rev. E* 76, 041304 (2007).

[19] Y. Shi and Y. Zhang, *Appl. Phys. A* 92, 621 (2008).

[20] H.J.H. Brouwers, *Phys. Rev. E* 78, 011303 (2008).

[21] K.W. Desmond and E.R. Weeks, *Phys. Rev. E* 80, 051305 (2009).

[22] I. Biazzo, F. Caltagirone, G. Parisi and F. Zamponi, *Phys. Rev. Lett.* 102, 195701 (2009).

[23] R.S. Farr and R.D. Groot, *J. Chem. Phys.* 131, 244104 (2009).

[24] M. Clusel, E.I., Corwin, A.O.N. Siemens and J. Brujić, *Nature* 460, 611 (2009).

[25] M. Danisch, Y. Bin and H.A. Makse, *Phys. Rev. E* 81, 051303 (2010).

[26] A.V. Kyrylyuk, A. Wouterse and A.P. Philipse, *Progr. Colloid Polym. Sci.* 137, 29 (2010).

[27] K.A. Newhall, I. Jorjadze, E. Vanden-Eijnden and J. Brujić, *Soft Matter* 7, 11518 (2011).

[28] A.B. Hopkins, F.H. Stillinger, S. Torquato, *Phys. Rev. E* 88, 022205 (2013).

[29] H.J.H. Brouwers, *Phys. Rev. E* 87, 032202 (2013).

[30] K.W. Desmond and E.R. Weeks, *Phys. Rev. E* 90, 022204 (2014).

[31] H. Ikeda, K. Miyazaki, H. Yoshino, A. Ikeda, *Phys. Rev. E* 103, 022613 (2021).

[32] H.J.H. Brouwers, *Physics – Uspekhi* 67, 510 (2024).

[33] L. Onsager, *Ann. N.Y. Acad. Sci.* 51, 627 (1949).

[34] Y.H. Yang and D.D. Wan, *Private communications* (2025).

[35] D.Y. Chen, Y. Jiao and S. Torquato, *J. Phys. Chem. B* 118, 7981 (2014).

[36] L. Meng, P. Lu, S. Li, J. Zhao, and T. Li, *T. Powder Technol.* 228, 284 (2012).

[37] J. A. Anderson, J. Glaser, and S. C. Glotzer, *Comput. Mater. Sci.* 173, 109363 (2020).

[38] K.W. Desmond, *Private communications* (2025).

[39] H.J.H. Brouwers, *Soft Matter* 19, 8465 (2023).

[40] A.P. Philipse, *Colloids Surf. A* 213, 167 (2003).

[41] G. Parisi and F. Zamponi, *J. Stat. Mech.: Theory Exp.*, P03017 (2006).

[42] K. Skoge, A. Donev, F.H. Stillinger and S. Torquato, *Phys. Rev. E* 74, 041127 (2006).

[43] B. Schmid and R. Schilling, *Phys. Rev. E* 81, 041502 (2010).

[44] H.J.H. Brouwers, *Phys. Rev. E* 89, 052211 (2014).

[45] H.Y. Sohn and C. Moreland, *Can. J. Chem. Eng.* 46, 162 (1968).